

Silicon isotopic fractionation of CAI-like vacuum evaporation residues

Kim B. Knight^{a,b,*}, Noriko T. Kita^d, Ruslan A. Mendybaev^{a,b}, Frank M. Richter^{a,b},
Andrew M. Davis^{a,b,c}, John W. Valley^d

^a Chicago Center for Cosmochemistry, The University of Chicago, Chicago, IL 60637, United States

^b Department of the Geophysical Sciences, The University of Chicago, Chicago, IL 60637, United States

^c Enrico Fermi Institute, The University of Chicago, Chicago, IL 60637, United States

^d WiscSIMS, Department of Geology and Geophysics, University of Wisconsin, Madison, WI 53706, United States

Received 19 June 2009; accepted in revised form 1 July 2009; available online 14 July 2009

Abstract

Calcium-, aluminum-rich inclusions (CAIs) are often enriched in the heavy isotopes of magnesium and silicon relative to bulk solar system materials. It is likely that these isotopic enrichments resulted from evaporative mass loss of magnesium and silicon from early solar system condensates while they were molten during one or more high-temperature reheating events. Quantitative interpretation of these enrichments requires laboratory determinations of the evaporation kinetics and associated isotopic fractionation effects for these elements. The experimental data for the kinetics of evaporation of magnesium and silicon and the evaporative isotopic fractionation of magnesium is reasonably complete for Type B CAI liquids (Richter F. M., Davis A. M., Ebel D. S., and Hashimoto A. (2002) Elemental and isotopic fractionation of Type B CAIs: experiments, theoretical considerations, and constraints on their thermal evolution. *Geochim. Cosmochim. Acta* **66**, 521–540; Richter F. M., Janney P. E., Mendybaev R. A., Davis A. M., and Wadhwa M. (2007a) Elemental and isotopic fractionation of Type B CAI-like liquids by evaporation. *Geochim. Cosmochim. Acta* **71**, 5544–5564.). However, the isotopic fractionation factor for silicon evaporating from such liquids has not been as extensively studied. Here we report new ion microprobe silicon isotopic measurements of residual glass from partial evaporation of Type B CAI liquids into vacuum. The silicon isotopic fractionation is reported as a kinetic fractionation factor, α_{Si} , corresponding to the ratio of the silicon isotopic composition of the evaporation flux to that of the residual silicate liquid. For CAI-like melts, we find that $\alpha_{\text{Si}} = 0.98985 \pm 0.00044$ (2σ) for $^{29}\text{Si}/^{28}\text{Si}$ with no resolvable variation with temperature over the temperature range of the experiments, 1600–1900 °C. This value is different from what has been reported for evaporation of liquid Mg_2SiO_4 (Davis A. M., Hashimoto A., Clayton R. N., and Mayeda T. K. (1990) Isotope mass fractionation during evaporation of Mg_2SiO_4 . *Nature* **347**, 655–658.) and of a melt with CI chondritic proportions of the major elements (Wang J., Davis A. M., Clayton R. N., Mayeda T. K., and Hashimoto A. (2001) Chemical and isotopic fractionation during the evaporation of the FeO–MgO–SiO₂–CaO–Al₂O₃–TiO₂–REE melt system. *Geochim. Cosmochim. Acta* **65**, 479–494.). There appears to be some compositional control on α_{Si} , whereas no compositional effects have been reported for α_{Mg} . We use the values of α_{Si} and α_{Mg} to calculate the chemical compositions of the unevaporated precursors of a number of isotopically fractionated CAIs from CV chondrites whose chemical compositions and magnesium and silicon isotopic compositions have been previously measured.

© 2009 Elsevier Ltd. All rights reserved.

1. INTRODUCTION

Calcium-, aluminum-rich inclusions (CAIs) in CV3 chondrites are the oldest objects known to have formed in the solar system, and they preserve a unique record of early

* Corresponding author. Present address: Lawrence Livermore National Laboratory, Livermore, CA 94550, United States. Tel.: +1 925 422 9396.

E-mail address: knight29@llnl.gov (K.B. Knight).

solar system conditions and processes. Interpreting this record requires laboratory data of various types. Traditional igneous petrology experiments are used to determine the melting behavior of CAI compositions and the textures produced by cooling of these liquids at various rates (Stolper, 1982; Stolper and Paque, 1986; Mendybaev et al., 2006). These experiments indicate that the large (several hundred μm) euhedral melilite grains characteristic of the Type B CAIs require that these CAIs experienced a high degree of partial melting (about 95% liquid), peak temperatures of about 1400 $^{\circ}\text{C}$, and cooling rates slower than 50 $^{\circ}\text{C h}^{-1}$. Faster cooling rates result in distinctly dendritic textures that are not observed in CAIs. Magnesium evaporation kinetics constrain the lower bound of CAI cooling rates to be not much less than 1 $^{\circ}\text{C h}^{-1}$ to prevent near-total loss of magnesium by evaporation (Richter et al., 2002).

Bulk compositions of Type B CAIs from CV3 chondrites show that they are depleted in magnesium, and perhaps silicon, relative to the expectations based on equilibrium condensation calculations done for plausible solar nebular pressures and temperatures (Grossman et al., 2000). These CAIs are often enriched in the heavy isotopes of magnesium and silicon by a few permil (Clayton et al., 1988; Grossman et al., 2008) and it seems likely that evaporative loss of magnesium and silicon led to the observed heavy isotope enrichment for these elements.

Laboratory experiments on kinetic isotope fractionation by evaporation relate the isotopic composition of an element in a residue to the amount of that element that has been evaporated. In the case of the Type B CAIs, silicon and magnesium are the most volatile of the major elements while calcium and aluminum are sufficiently refractory that they do not evaporate to any significant degree until all the magnesium has been lost. The keys to restoring the original, preevaporation, composition of a CAI with fractionated silicon and magnesium isotopes are the kinetic isotope fractionation factors $\alpha_{\text{Mg}} = ({}^{25}\text{Mg}/{}^{24}\text{Mg})_{\text{flux}}/({}^{25}\text{Mg}/{}^{24}\text{Mg})_{\text{residue}}$ and $\alpha_{\text{Si}} = ({}^{29}\text{Si}/{}^{28}\text{Si})_{\text{flux}}/({}^{29}\text{Si}/{}^{28}\text{Si})_{\text{residue}}$, where “flux” refers to the material evaporating from the residue and “residue” refers to the still-condensed material. If these kinetic fractionation factors are effectively independent of the evolving composition of the residue liquid, the residue remains isotopically homogeneous, and the evaporated material is continuously isolated from exchange with the residue, then the relationship between the isotopic fractionation of an element in the residue and the fraction of that element remaining in the residue takes the form of a Rayleigh fractionation equation. The relevant Rayleigh equation for isotopic fractionation by evaporation is:

$$\frac{R}{R_0} = f_{iX}^{\alpha_X - 1}, \quad (1)$$

where $R = ({}^i\text{X}/{}^j\text{X})_{\text{residue}}$, $R_0 = ({}^i\text{X}/{}^j\text{X})_{\text{preevaporation}}$, ${}^i\text{X}$ and ${}^j\text{X}$ are the isotopes i and j of element X, f_{iX} is the fraction of ${}^i\text{X}$ remaining in the residue, and α_X is the kinetic isotope fractionation factor for isotopes of element X (see Richter (2004)). If Eq. (1) can be validated by laboratory experiments for all volatilized elements of interest, one will then have a tool with which to calculate the original composition of evaporation residues. If the Type B CAIs are evapora-

tion residues, the information required to determine their original bulk composition is their present silicon and magnesium isotopic composition, an estimate of their preevaporation magnesium and silicon isotopic composition, a representative analysis of their present bulk silicon and magnesium elemental concentrations, and the kinetic isotope fractionation factors α_{Mg} and α_{Si} .

It is widely accepted that the Type B CAIs are evaporation residues because of the correlation of the silicon and magnesium isotopic fractionations (e.g., Clayton et al., 1988; Grossman et al., 2008), which is a typical characteristic of evaporation residues of silicate liquids (Davis et al., 1990). The usual assumption for the silicon and magnesium isotopic composition of the Type B CAIs prior to evaporation is that it is the same as that of typical bulk solar system rocky material as represented by chondritic meteorites (see Davis and Richter (2007), and references therein). This assumption is consistent with the observation that when the silicon and magnesium isotopic fractionations of the Type B CAIs are measured relative to chondritic meteorites they form a trend in a plot of silicon versus magnesium fractionations that, within the scatter of the data, passes through the origin.

Kinetic isotope fractionation factors for silicon and magnesium are essential for determining the composition of the preevaporation precursor of a given Type B CAI. The kinetic isotope fractionation factor for magnesium evaporating from a Type B CAI-like liquid into vacuum has been determined for a range of evaporation temperatures (1600–1900 $^{\circ}\text{C}$) and for evaporation into 2×10^{-4} bars H_2 at 1500 $^{\circ}\text{C}$ (Richter et al., 2002, 2007a, 2008). In contrast to this rather extensive data set for magnesium, there exists only a preliminary report for α_{Si} derived from silicon isotopic measurements made by laser ablation multicollector inductively coupled plasma mass spectrometry (LA-MC-ICPMS) of vacuum-evaporated CAI-like liquids (Janney et al., 2005). A potential problem with the LA-MC-ICPMS measurements is that no corrections were made for possible variations in instrumental mass fractionation with sample composition. These matrix corrections might be significant, given the large range in chemical composition among the starting material and various evaporation residues. Another source of concern is that the α_{Si} value reported by Janney et al. (2005) for the CAI-like liquid was significantly different from values that had been reported for melts of forsterite composition (Davis et al., 1990), molten Allende meteorite (Floss et al., 1996), and for a liquid with initially solar proportions of the major element oxides (Wang et al., 2001).

Here we report new silicon isotopic fractionation data measured using an ion microprobe to analyze a subset of the evaporation residues for which Richter et al. (2007a) reported magnesium isotopic fractionations. The starting composition was CAI-like and this material was evaporated into vacuum at temperatures of 1600, 1800, and 1900 $^{\circ}\text{C}$, well above the melting point. Development of methods for silicon isotope measurements using a multicollector ion microprobe provided the advantages of sufficient mass resolution to resolve ${}^{28}\text{Si}$, ${}^{29}\text{Si}$ and ${}^{30}\text{Si}$, as well as ${}^{27}\text{Al}$, from potential isobaric interferences with spatial resolution of a

few μm to assess any internal isotopic zoning of run products. We were also able to evaluate possible compositional influences on measured isotopic data.

2. EXPERIMENTAL AND ANALYTICAL TECHNIQUES

A series of $\text{CaO-MgO-Al}_2\text{O}_3\text{-SiO}_2$ (CMAS) samples were evaporated in a vacuum furnace (Hashimoto, 1990) at total pressures of less than 10^{-9} bars (Richter et al., 2007a). The starting material for these experiments was somewhat richer in MgO and SiO_2 than typical Type B CAIs, in order to attain Type B CAI composition when sufficiently evaporated. Starting glass containing 46.00 wt% SiO_2 , 19.39% Al_2O_3 , 11.48% MgO, and 23.12% CaO was loaded into 2.5 mm diameter iridium wire loops and each sample was evaporated individually: the sample was introduced into the furnace at room temperature, the furnace was pumped down and then the temperature was slowly raised to 1400 °C. Once the pressure in the furnace fell below 10^{-9} bars, the temperature was raised to 1600 °C (at 20 °C min^{-1}), 1800 °C (at 20 °C min^{-1}) or 1900 °C (at 40 °C min^{-1} from 1600 °C), held for a predetermined period of time, and then quenched by cutting power to the heating element (see Richter et al. (2007a), for further details). In all but one case (R3-09 evaporated at 1900 °C), the samples quenched to chemically, and as we show later, isotopically uniform glasses. Residue R3-09 is microcrystalline, and reliable analyses could not be obtained. The chemical compositions of all materials used in this study were determined using a JEOL JSM-5800LV scanning electron microscope equipped with an Oxford/Link ISIS-300 energy-dispersive X-ray microanalysis system. All analyses were done with a 15 keV accelerating voltage, a beam current of ~ 0.5 nA, and were standardized with a variety of natural and synthetic minerals. The compositions of the evaporation residues used in this study were originally reported in Richter et al. (2007a), and are listed in Table 1. For isotopic analysis, fragments of these glasses were mounted in epoxy with an internal running standard, CMAS-0, very similar in composition to the starting material.

Silicon isotopic measurements were made with a Cameca IMS-1280 multicollector ion microprobe at the University of Wisconsin (WiscSIMS), using a Cs^+ primary ion beam and negative secondary ions. We also investigated using an $^{16}\text{O}^-$ primary beam and positive secondary ions, but found that negative secondary ions gave a higher ion yield and less instrumental mass fractionation than positive ones. The analysis conditions for silicon isotopic analysis are generally similar to those for high precision oxygen isotopic analysis (Page et al., 2007; Kita et al., 2009). The Cs^+ primary beam was operated at a current of 5 nA focused to a beam diameter of ~ 10 μm and an electron flood gun was used for the charge compensation. The settings for secondary ion optics include: 200 times magnification at the transfer optics; an entrance slit width of 90 μm ; a 4000 μm square field aperture; and an energy window of 40 eV. Three silicon isotopes ($^{28}\text{Si}^-$, $^{29}\text{Si}^-$, $^{30}\text{Si}^-$), along with $^{27}\text{Al}^-$, were detected simultaneously with multicollection Faraday cups at a mass resolving power (MRP; width of

the mass spectrum at 10% height) of 2200. In this condition, the contribution of $^{28}\text{SiH}^-$ to $^{29}\text{Si}^-$ (corresponding to $\text{MRP} = 3500$) was found to be negligibly small ($< 0.1\%$) assuming that hydride and atomic mass peaks have the same shapes (the tail of the $^{29}\text{Si}^-$ signal was ≤ 50 ppm at 0.084 amu below the peak center, equivalent to the mass difference between $^{29}\text{Si}^-$ and $^{28}\text{SiH}^-$) and typical $^{28}\text{SiH}^-/^{29}\text{Si}^-$ ratios during the measurements were ~ 0.1 . The secondary $^{28}\text{Si}^-$ ion intensity ranges between 4×10^7 and 1×10^8 cps, depending on the SiO_2 content of the sample. Single analyses took ~ 4 min per spot, including pre-sputtering (30 s), automatic centering of the secondary beam (~ 1 min) and signal collection (80 s). Count rates for Si^- ions did not change significantly over the course of an analysis. Signal intensities of all isotopes changed by $< 5\%$ from the first to the last cycle of a run. Over the duration of the two separate analytical sessions, the ^{28}Si count rate on the running standard CMAS-0 remained constant within $\pm 5\%$.

In contrast to the isotope measurements of Janney et al. (2005) by LA-MC-ICPMS, which could only measure $^{28}\text{Si}^+$ and $^{29}\text{Si}^+$ because of an isobaric interference of $^{14}\text{N}^{16}\text{O}^+$ on $^{30}\text{Si}^+$, we were able to use four static Faraday cups for simultaneous determination of $^{28}\text{Si}^-$, $^{29}\text{Si}^-$, $^{30}\text{Si}^-$ and $^{27}\text{Al}^-$. Measuring $^{27}\text{Al}^-$ along with the silicon isotopes provided an independent measure of the elemental compositions, which compared well with the SEM-derived composition measurements. Multiple spots were analyzed in each sample, interspersed with multiple spot analyses of the internal running standard CMAS-0, a chip of which was mounted on each sample or CMAS matrix-correction glass mount. Correction of the samples for variations within and between runs can be made in two ways: (1) normalize each data point to the average of bracketing CMAS-0 analyses; (2) normalize each data point to the average for the CMAS-0 standard for that run, where a run is defined as a series of analyses without sample exchange or major tuning of the instrument. We found that either method gave similar data, but the second option gave slightly more precise results.

Silicon isotopic data measured on each sample and normalized to the CMAS-0 standard are reported as δ values in Table 1 in the columns labeled “measured”. External reproducibility is 0.32 ‰ for $\delta^{29}\text{Si}$ and 0.52 ‰ for $\delta^{30}\text{Si}$ (2σ), based on the standard deviation of 146 spot analyses of the CMAS-0 standard. These errors are somewhat correlated, as the external reproducibility for $\Delta^{29}\text{Si}$, defined as $\delta^{29}\text{Si} - 0.5 \times \delta^{30}\text{Si}$, is only 0.25‰. Four to twelve spot analyses were made of each sample or CMAS matrix-correction glass (CMAS-1 to -13). The standard error and the external reproducibility divided by the square root of the number of spot analyses (all 2σ) were compared and the larger of the two (usually the latter) was reported for each analysis in Table 1.

Variations in instrumental mass fractionation (IMF, by which we mean the difference between true silicon isotope ratios and those measured by the instrument) due to variations in chemical composition are known for a number of elements, but are especially large for silicon. Such variations are often referred to as “matrix effects” and we will

Table 1

Chemical and isotopic compositions of evaporation residues and matrix-correction standards. Uncertainties are 2σ and are based on the larger of the internal and external precisions.

Sample	Run temp (°C)	MgO (wt%)	SiO ₂ (wt%)	Al ₂ O ₃ (wt%)	CaO (wt%)	²⁸ Si loss ^a (%)	# Spots	²⁷ Al ⁻ / ²⁸ Si ^{-b}	^{δ²⁹Si} (‰) ^c	^{δ³⁰Si} (‰) ^c	^{δ²⁹Si} (‰)	^{δ³⁰Si} (‰)	^{δ²⁵Mg} (‰) ^d
									Measured	Matrix-corrected	Matrix-corrected	Matrix-corrected	
CMAS-0		10.79	46.82	19.09	23.30		146	≡1.000	≡0.000	≡0.000	≡0.000	≡0.000	
CMAS-1		0.33	17.41	35.98	46.28		9	3.970 ± 0.033	3.01 ± 0.11	6.05 ± 0.18	-0.19 ± 0.21	-0.22 ± 0.35	
CMAS-2		1.07	22.05	32.56	44.32		9	2.976 ± 0.025	2.60 ± 0.11	5.15 ± 0.17	0.05 ± 0.18	0.14 ± 0.30	
CMAS-3		5.05	26.35	28.81	39.80		9	2.381 ± 0.020	1.73 ± 0.11	3.33 ± 0.17	-0.21 ± 0.16	-0.47 ± 0.26	
CMAS-4		8.78	32.27	26.09	32.86		9	1.836 ± 0.015	1.50 ± 0.11	2.83 ± 0.17	0.19 ± 0.14	0.26 ± 0.24	
CMAS-4 + 5		10.58	38.43	21.61	29.39		9	1.347 ± 0.011	0.91 ± 0.11	1.76 ± 0.17	0.33 ± 0.14	0.61 ± 0.23	
CMAS-5		11.90	45.41	18.51	24.18		9	1.005 ± 0.008	0.26 ± 0.11	0.40 ± 0.17	0.26 ± 0.15	0.40 ± 0.24	
CMAS-6		11.34	38.98	21.91	27.77		9	1.366 ± 0.011	0.88 ± 0.11	1.27 ± 0.17	0.30 ± 0.14	0.13 ± 0.23	
CMAS-7 ^e		0.05	10.64	40.35	48.96		8	7.880 ± 0.070	4.10 ± 0.19	7.08 ± 0.18	-0.08 ± 0.31	-1.10 ± 0.43	
CMAS-8		0.15	20.97	35.32	43.56		9	3.474 ± 0.029	3.02 ± 0.11	5.70 ± 0.17	0.20 ± 0.19	0.19 ± 0.32	
CMAS-9		9.07	35.29	24.77	30.86		9	1.683 ± 0.014	1.00 ± 0.11	1.92 ± 0.21	-0.02 ± 0.14	-0.08 ± 0.26	
CMAS-10		10.22	41.24	21.71	26.83		9	1.295 ± 0.011	0.55 ± 0.11	1.02 ± 0.17	0.09 ± 0.14	0.12 ± 0.23	
CMAS-12		4.09	30.08	29.37	36.46		9	2.204 ± 0.018	2.01 ± 0.14	3.86 ± 0.25	0.31 ± 0.18	0.52 ± 0.31	
CMAS-13		9.78	46.60	19.54	24.08		8	1.030 ± 0.009	0.17 ± 0.19	0.05 ± 0.18	0.12 ± 0.15	-0.04 ± 0.24	
Starting composition		11.48	46.00	19.39	23.12	≡0.00							
R3-2	1600	12.22	46.36	19.31	22.11	-1.21 ± 0.10	8	1.053 ± 0.009	-0.38 ± 0.11	-0.69 ± 0.18	-0.42 ± 0.15	-0.76 ± 0.24	-0.105 ± 0.014
R3-1	1600	9.62	33.93	26.24	30.21	45.53 ± 0.30	4	1.833 ± 0.023	6.51 ± 0.16	13.06 ± 0.26	5.29 ± 0.19	10.67 ± 0.30	6.188 ± 0.006
R3-21	1600	9.44	33.69	26.32	30.54	46.08 ± 0.34	4	1.877 ± 0.024	6.83 ± 0.23	13.18 ± 0.31	5.59 ± 0.25	10.75 ± 0.35	
R3-19	1600	6.70	31.34	28.86	33.11	54.26 ± 0.25	4	2.162 ± 0.027	8.39 ± 0.16	16.90 ± 0.26	6.80 ± 0.19	13.80 ± 0.31	11.887 ± 0.042
R3-20	1600	6.43	31.01	29.11	33.45	55.13 ± 0.24	4	2.179 ± 0.027	8.84 ± 0.19	17.46 ± 0.26	7.22 ± 0.22	14.29 ± 0.31	12.337 ± 0.053
R3-18	1600	4.34	29.39	30.81	35.46	59.83 ± 0.21	8	2.327 ± 0.021	10.53 ± 0.14	20.89 ± 0.24	8.68 ± 0.18	17.27 ± 0.31	17.946 ± 0.023
R3-4	1600	4.60	30.84	30.20	34.36	56.99 ± 0.24	12	2.159 ± 0.016	10.52 ± 0.15	20.66 ± 0.19	8.81 ± 0.18	17.31 ± 0.26	19.861 ± 0.023
R3-8	1600	1.65	26.73	33.21	38.40	66.11 ± 0.19	4	2.612 ± 0.033	12.88 ± 0.16	25.22 ± 0.26	10.67 ± 0.21	20.91 ± 0.34	32.359 ± 0.016
R3-7	1600	0.20	22.40	36.01	41.39	73.82 ± 0.16	4	3.402 ± 0.043	15.96 ± 0.20	31.01 ± 0.32	13.23 ± 0.25	25.68 ± 0.41	
R3-5	1600	0.12	17.74	38.36	43.78	80.54 ± 0.16	4	4.501 ± 0.057	19.50 ± 0.24	37.98 ± 0.39	16.22 ± 0.31	31.55 ± 0.50	
R-3	1800	11.82	38.87	22.55	26.76	27.36 ± 0.34	8	1.433 ± 0.013	3.36 ± 0.11	6.80 ± 0.18	2.71 ± 0.14	5.54 ± 0.23	1.723 ± 0.009
R-2	1800	10.07	33.58	25.72	30.63	45.01 ± 0.25	7	1.834 ± 0.017	6.51 ± 0.12	12.92 ± 0.20	5.31 ± 0.15	10.57 ± 0.25	5.494 ± 0.044
R-18	1800	5.20	28.05	30.51	36.24	61.28 ± 0.24	8	2.457 ± 0.022	10.99 ± 0.11	21.44 ± 0.22	9.06 ± 0.16	17.67 ± 0.29	17.059 ± 0.032
R3-14	1800	3.12	26.13	31.76	38.98	65.36 ± 0.29	7	2.649 ± 0.025	13.03 ± 0.12	25.11 ± 0.24	10.88 ± 0.18	20.88 ± 0.32	25.372 ± 0.031
R2-1	1800	0.19	19.91	36.53	43.38	77.06 ± 0.15	9	3.744 ± 0.031	17.62 ± 0.13	34.67 ± 0.17	14.64 ± 0.22	28.83 ± 0.33	69.148 ± 0.063
R3-12	1900	11.37	44.53	19.26	24.84	2.55 ± 0.56	8	1.109 ± 0.010	0.92 ± 0.11	1.78 ± 0.18	0.82 ± 0.15	1.58 ± 0.24	
R3-10	1900	9.13	31.52	26.86	32.48	50.57 ± 0.29	11	2.027 ± 0.015	8.36 ± 0.10	16.31 ± 0.16	6.94 ± 0.14	13.53 ± 0.23	8.135 ± 0.007
R3-11	1900	3.33	25.24	32.35	39.09	67.15 ± 0.19	4	2.480 ± 0.031	13.61 ± 0.12	26.27 ± 0.35	11.34 ± 0.21	21.84 ± 0.41	25.810 ± 0.020
R3-9	1900	1.04	21.81	35.06	42.08	73.81 ± 0.23	9	3.339 ± 0.028	15.85 ± 0.12	31.30 ± 0.26	13.13 ± 0.20	25.97 ± 0.36	43.265 ± 0.017
R3-15	1900	0.80	21.10	35.10	43.10	74.70 ± 0.10	4	3.104 ± 0.039	17.31 ± 0.17	33.65 ± 0.26	14.52 ± 0.23	28.18 ± 0.37	47.733 ± 0.023
R3-13	1900	0.09	17.76	37.08	45.05	79.84 ± 0.13	4	4.132 ± 0.052	19.02 ± 0.24	37.21 ± 0.38	15.80 ± 0.30	30.91 ± 0.48	

^a Determined from SiO₂/Al₂O₃ ratio measured by SEM/EDX and from matrix-corrected silicon isotopic composition.^b Measured by MC-SIMS and normalized to CMAS-0.^c $\delta^{29}\text{Si} = [({}^{29}\text{Si}/{}^{28}\text{Si})_{\text{sample}}/({}^{29}\text{Si}/{}^{28}\text{Si})_{\text{std}} - 1] \times 1000$; $\delta^{30}\text{Si} = [({}^{30}\text{Si}/{}^{28}\text{Si})_{\text{sample}}/({}^{30}\text{Si}/{}^{28}\text{Si})_{\text{std}} - 1] \times 1000$.^d Richter et al. (2007).^e This CMAS standard glass is an outlier on a plot of ²⁹Si vs. ³⁰Si (Fig. 2 inset) and was not included in determination of the matrix-correction.

use that term here. The matrix effect for silicon isotopes in CMAS glasses was calibrated using a set of specially made isotopically unfractionated glasses with bulk chemical compositions similar to those of the evaporation residues (Table 1). CMAS matrix-correction glasses were prepared from mixtures of CaCO_3 , MgO , Al_2O_3 , and SiO_2 . These mixtures were decarbonated at 1000°C and melted in a 1 atm furnace at $T \sim 1550^\circ\text{C}$ for 36–48 h in air, followed by quenching in water. The CMAS standards produced in this way were found to be chemically and isotopically homogeneous. The MgO and SiO_2 contents of the glasses used for matrix corrections are compared with those of the evaporation residues in Fig. 1. The silicon isotopic data for the matrix-correction glasses were collected in the same manner and at the same time as those for the evaporation residues. In order to correct data on evaporation residues for matrix effects, we examined the relationship between a number of compositional parameters and silicon isotopic composition. The ratio $\text{SiO}_2/(\text{Al}_2\text{O}_3 + \text{SiO}_2)$ with oxides in wt% (measured by SEM–EDX) came closest to a linear relationship (Fig. 2) and we used this ratio to correct the measured silicon isotopic composition of the evaporation residues for matrix compositional effects on isotope ratio measurements. The regression through the data plotted in Fig. 2 has some uncertainty due to scatter about the regression line and the 2σ error envelope is shown. This uncertainty was propagated with the uncertainty in the measured $\delta^{29}\text{Si}$ and $\delta^{30}\text{Si}$ values and reported for the “matrix-corrected” values in Table 1. The evaporation residues span a large range of compositions, necessitating corrections up to 3.3‰ for $\delta^{29}\text{Si}$ and 6.4‰ for $\delta^{30}\text{Si}$, and underscoring the importance of appropriate matrix corrections when making SIMS determinations of silicon isotope compositions. The corrections applied to each sample and CMAS matrix-correction glass are shown in a $\delta^{29}\text{Si}$ vs. $\delta^{30}\text{Si}$ plot that is an inset in Fig. 2. One CMAS glass, CMAS-7, is a clear outlier with an excess in $\delta^{29}\text{Si}$ (or a deficit in $\delta^{30}\text{Si}$). This effect was consistent among the eight spot analyses of CMAS-7, but was not seen in any other sample. We have no explanation for this effect, but did not use this sample in the regressions

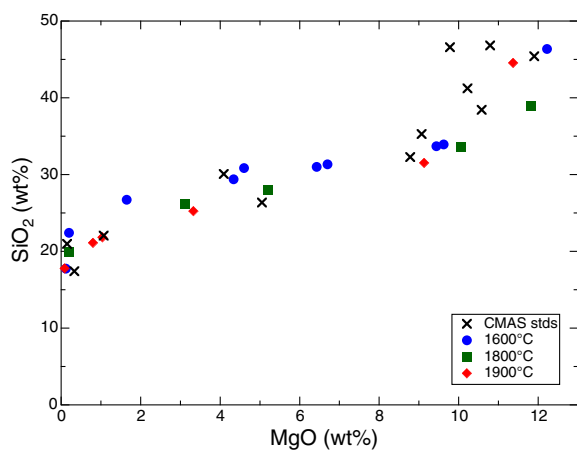


Fig. 1. SiO_2 vs. MgO contents of evaporation residues and of CMAS glasses used for correction of matrix effects in silicon isotopic measurement. Uncertainties are smaller than the symbols.

shown in Fig. 2. After correction for matrix effects, the CMAS matrix-correction glasses have external reproducibilities of 0.36 and 0.59‰ (2σ) for $\delta^{29}\text{Si}$ and $\delta^{30}\text{Si}$, respectively. These values are not significantly different from the external reproducibilities derived from CMAS-0, and show that the matrix-correction we applied is quite effective and does not significantly increase uncertainties.

For large fractionation effects such as these, however, it is more appropriate to plot $1000 \ln(R/R_0)$ values for ^{29}Si vs. those for ^{30}Si , where $R/R_0 = (^{29}\text{Si}/^{28}\text{Si})_{\text{sample}} / (^{29}\text{Si}/^{28}\text{Si})_{\text{std}} = \delta^{29}\text{Si} / 1000 + 1$ for ^{29}Si , because exponential processes such as Rayleigh fractionation are linear on such plots. Such a plot is shown in Fig. 3; a weighted regression through the data, calculated with Model 1 of Isoplot (Ludwig, 1992), yields a slope of 0.5179 ± 0.0056 , an intercept of -0.09 ± 0.10 (2σ), and a mean square weighted deviation (MSWD) of 0.87 .

3. ASSESSMENT OF RAYLEIGH FRACTIONATION AND THE KINETIC ISOTOPE FRACTIONATION FACTOR FOR SILICON

Table 1 shows all chemical and isotopic data for matrix-correction glasses and evaporation residue samples. The amount of silicon lost by each residue relative to the starting composition was calculated using the $\text{SiO}_2/\text{Al}_2\text{O}_3$ ratio measured by SEM–EDX, assuming that Al_2O_3 is sufficiently refractory that it does not evaporate. CaO is also much more refractory than either MgO or SiO_2 , but less refractory than Al_2O_3 and there is no indication that it evaporated. Although there is a little scatter in the $\text{CaO}/\text{Al}_2\text{O}_3$ ratio (the standard deviation of the $\text{CaO}/\text{Al}_2\text{O}_3$ ratio for all residues is $\sim 3\%$ of the ratio), there is no correlation between the $\text{CaO}/\text{Al}_2\text{O}_3$ ratio and the $\text{SiO}_2/\text{Al}_2\text{O}_3$ ratio of the evaporation residues. The fraction of silicon lost by each sample, together with the relative abundance of the silicon isotopes, was used to calculate $f_{28\text{Si}}$, the fraction of ^{28}Si remaining in the residue. Fig. 4 shows silicon isotopic composition versus percent ^{28}Si evaporated for all evaporation residues. Also shown are two curves for the $\delta^{29}\text{Si}$ and $\delta^{30}\text{Si}$ calculated using Eq. (1) (*i.e.*, assuming Rayleigh fractionation) and a kinetic isotope fractionation factor calculated as $\alpha_{29\text{Si}} = \sqrt{\text{M.W.}(^{28}\text{SiO})/\text{M.W.}(^{29}\text{SiO})}$ and $\alpha_{30\text{Si}} = \sqrt{\text{M.W.}(^{28}\text{SiO})/\text{M.W.}(^{30}\text{SiO})}$, where M.W. values are the molecular weights of the relevant species. SiO is the dominant gas species that would be in equilibrium with the silicate melt, both from mass spectrometry of the gas composition evaporated from molten Mg_2SiO_4 (Nichols et al., 1995) and from equilibrium thermodynamic calculations (Nagahara and Ozawa, 1996; Wang et al., 1999; Grossman et al., 2000). The practice of calculating values for isotope fractionation factors based on the inverse square root of the mass of the dominant gas species is commonly used in the absence of actual experimental data. The data lie close to but not exactly along the calculated curves, indicating that the actual values of the kinetic isotope fractionation factors are somewhat closer to 1 than the calculated values.

The best way to test whether isotopic fractionation of silicon during evaporation is consistent with Rayleigh frac-

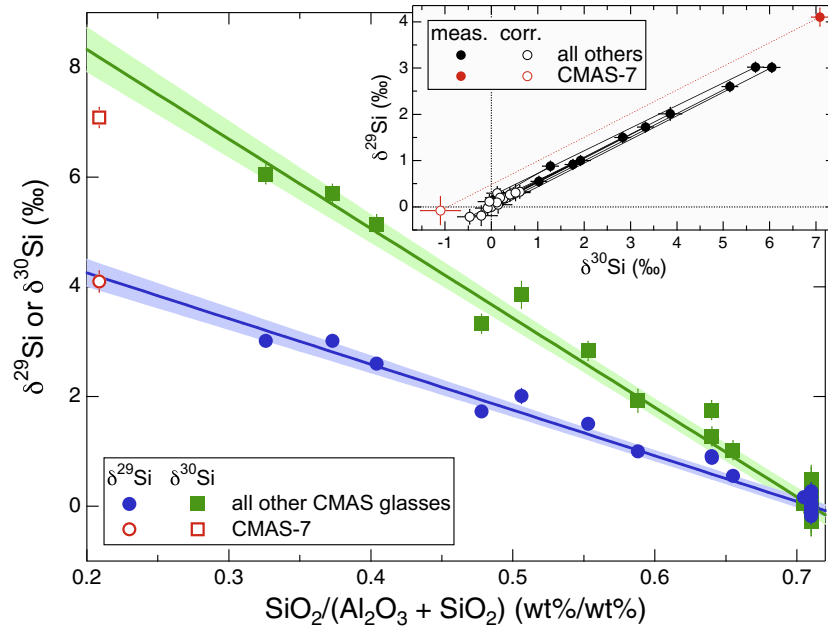


Fig. 2. Measured $\delta^{29}\text{Si}$ and $\delta^{30}\text{Si}$ in CMAS glass standards as a function of $\text{SiO}_2/(\text{SiO}_2 + \text{Al}_2\text{O}_3)$. Uncertainties are 2σ . All of the glasses have the same silicon isotopic composition and the variations in measured values reflect the dependence of instrumental mass fractionation on chemical composition. The inset shows $\delta^{29}\text{Si}$ vs. $\delta^{30}\text{Si}$ for measured and corrected CMAS glass standards. The data point for CMAS-7 has high $\delta^{29}\text{Si}$ relative to $\delta^{30}\text{Si}$ and were not included in the regressions shown in main part of the figure.

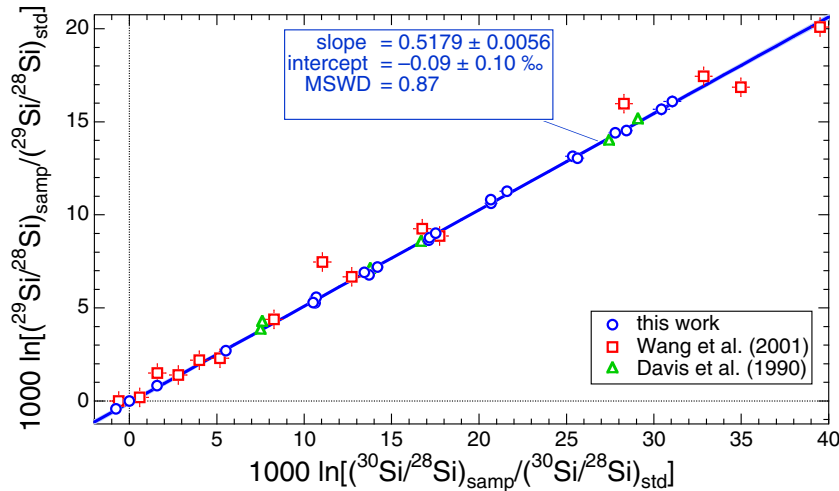


Fig. 3. $1000 \ln(R/R_0)$ for ^{29}Si vs. ^{30}Si for matrix-corrected silicon isotopic compositions of CMAS evaporation residues; also shown are evaporation experiments on liquid Mg_2SiO_4 (Davis et al., 1990) and on melts of initially CI chondritic proportions of major element oxides (Wang et al., 2001). Uncertainties are 2σ . It is more conventional to plot $\delta^{29}\text{Si}$ vs. $\delta^{30}\text{Si}$, but for such large isotopic fractionation effects, exponential fractionation processes such as Rayleigh fractionation are straight lines on log–log plots (and are curves on δ – δ plots). The regression shown applies only to the data of this work.

tionation is to plot $\ln(R/R_0)$ against $-\ln f_{28\text{Si}}$, where R is the isotopic ratio of the residue and R_0 is that of the starting composition. By taking the natural logarithm of both sides of Eq. (1) we establish that

$$\ln(R/R_0) = -(1 - \alpha) \ln f_{28\text{Si}}. \quad (2)$$

Data obeying Rayleigh fractionation with constant α should lie on a straight line of slope $1 - \alpha$ in a plot of

$\ln(R/R_0)$ against $-\ln f_{28\text{Si}}$. Fig. 5 shows that data for evaporation experiments at all three run temperatures fall along single straight lines with slopes corresponding to $\alpha_{29\text{Si}} = 0.98985 \pm 0.00044$ and $\alpha_{30\text{Si}} = 0.98045 \pm 0.00074$ (2σ). Individual temperature experiments yield indistinguishable slopes, with $\delta^{29}\text{Si}$, $\alpha_{1600\text{C}} = 0.98978 \pm 0.00062$, $\alpha_{1800\text{C}} = 0.98952 \pm 0.00074$, $\alpha_{1900\text{C}} = 0.99032 \pm 0.00070$, and for $\delta^{30}\text{Si}$, $\alpha_{1600\text{C}} = 0.98037 \pm 0.00106$, $\alpha_{1800\text{C}} = 0.97986 \pm 0.00102$,

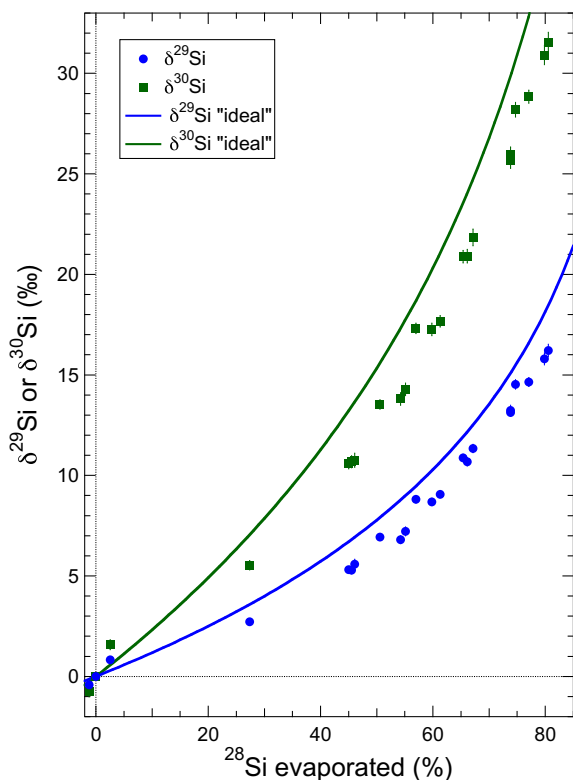


Fig. 4. Silicon isotope compositions of evaporated residues vs. percent ^{28}Si evaporated. Uncertainties are 2σ . Also shown are curves for Rayleigh fractionation using $\alpha_{29\text{Si}} = \sqrt{M.W.^{28}\text{SiO}/M.W.^{29}\text{SiO}}$ and $\alpha_{30\text{Si}} = \sqrt{M.W.^{28}\text{SiO}/M.W.^{30}\text{SiO}}$, labeled “ideal”. The data lie significantly below the “ideal” curves, indicating that the α values are closer to one than simple theory would lead one to expect.

$\alpha_{1900\text{C}} = 0.98122 \pm 0.00114$. Using a weighted regression (Model 1 fit of Isoplot, Ludwig, 1992) gives rather high MSWD values above 20 for all of the regressions in Fig. 5, indicating that the data scatter by more than would be expected from the uncertainties in the individual data points. For this reason, Isoplot Model 2 was used, in which the uncertainty in the regression is controlled by the scatter of the data points rather than their individual uncertainties. The fits we used to determine the values for $\alpha_{29\text{Si}}$ and $\alpha_{30\text{Si}}$ were not forced through the origin, but the intercepts are within error of the origin. There is some scatter to the data, but α does not appear to depend on temperature (see below). If $\alpha_{29\text{Si}}$ and $\alpha_{30\text{Si}}$ were dependent on composition, the data in Fig. 5 might be better described by curves rather than straight lines (because the chemical composition evolves with degree of evaporation), but there is no hint of a need to fit anything other than straight lines. Data for vacuum evaporation of Mg_2SiO_4 melts (Davis et al., 1990) and melts with initially chondritic proportions of major element oxides (Wang et al., 2001); for these, regressions were calculated in the same way as for the CMAS experiments, with Isoplot Model 2 and without forcing the regressions through the origin. None of the CMAS evaporation residues showed any sign of a relationship between isotopic composition and distance from the evaporating surface.

Fig. 6 demonstrates this lack of internal isotopic zoning for three residues.

Our estimate of $\alpha_{29\text{Si}} = 0.98985 \pm 0.00044$ is essentially the same as the value reported by Janney et al. (2005), 0.9898 ± 0.0004 . In that work, laser ablation multicollector inductively coupled plasma mass spectrometry (LA-MC-ICPMS) was used to measure $^{29}\text{Si}/^{28}\text{Si}$ ratios of five samples from the same series of 1800 °C residues for which we present ion microprobe data here (those authors did not report $^{30}\text{Si}/^{28}\text{Si}$ ratios, because of a significant interference of $^{14}\text{N}^{16}\text{O}^+$ on $^{30}\text{Si}^+$). This agreement is surprising considering that no matrix corrections were applied to the Janney et al. (2005) measurements, whereas in the case of our ion microprobe measurements matrix corrections of several ‰ were made. A comparison of advantages and complications of SIMS and ICPMS techniques for silicon isotopes is given in Basile-Doelsch et al. (2005). The good agreement between our results and those of Janney et al. (2005) suggest that there is little matrix effect in LA-MC-ICPMS, at least for CMAS glasses. SIMS offers several advantages over both LA-MC-ICPMS and solution MC-ICPMS (in which bulk samples are dissolved and chemically purified) analyses, despite the need for careful characterization and monitoring of matrix effects. These include resolution of a number of potential isobaric interferences resulting in additional isotopic information and analytical confidence, as well as the ability to perform *in situ* analyses with spatial resolution of a few μm .

4. DISCUSSION

4.1. Isotope fractionation factors

In Fig. 7, we compare the kinetic isotope fractionation factors for a CAI-like liquid at our three run temperatures in vacuum to values reported in earlier studies by Davis et al. (1990) for liquid Mg_2SiO_4 , and by Wang et al. (2001) for a liquid with initially CI chondritic proportions of the major oxides. We do not show data by Floss et al. (1996) for molten Allende meteorite, as that experiment appears to have suffered from recondensation effects. Furthermore, Floss et al. (1996) apparently did not correct for compositional effects on IMF, which we have shown are quite important in SIMS analysis of silicon isotopes. Shown for reference are the values $\alpha_{29\text{Si}} = \sqrt{M.W.^{(28}\text{SiO})/M.W.^{(29}\text{SiO})}$ and $\alpha_{30\text{Si}} = \sqrt{M.W.^{(28}\text{SiO})/M.W.^{(30}\text{SiO})}$ that are commonly used in the absence of relevant experimental data. The main conclusions that can be drawn from Fig. 7 are that α_{Si} values are relatively insensitive to the evaporation temperature but seem to depend on the composition of the evaporating liquid. None of the three sets of experiments plotted in Fig. 7 show any resolvable temperature dependence of α_{Si} values. On the other hand, a compositional dependence of $\alpha_{29\text{Si}}$ is clearly seen with the average $\alpha_{29\text{Si}} = 0.98985 \pm 0.00044$ and $\alpha_{30\text{Si}} = 0.98045 \pm 0.00074$ for CAI-like liquids being furthest from 1 and thus corresponding to the greatest silicon isotope fractionation for a given amount of silicon evaporated, to $\alpha_{29\text{Si}} = 0.99271 \pm 0.00092$ and $\alpha_{30\text{Si}} = 0.98577 \pm 0.00180$ for melts of forsterite composition. We cannot, however, completely rule out the effect of the sample size on the silicon

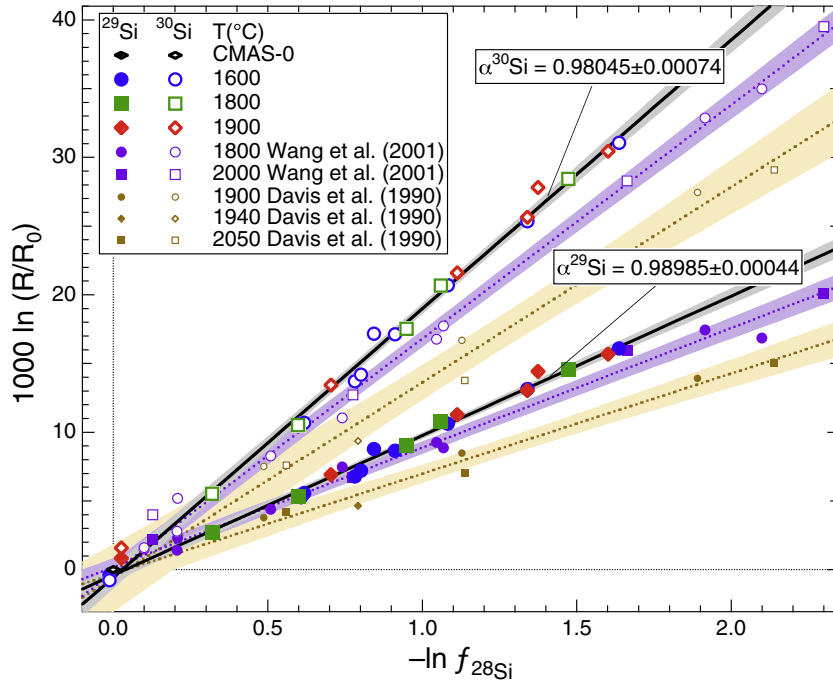


Fig. 5. $1000 \ln(R/R_0)$ vs. $-\ln f_{28\text{Si}}$. Uncertainties are 2σ . The slopes in this plot are equal to $1000(1 - \alpha)$ and include data from experiments at all run temperatures. Linear regressions are shown for ^{29}Si and ^{30}Si , with 2σ error bounds determined from the scatter of the data about the lines. Also shown are data and regressions for Mg_2SiO_4 melts (Davis et al., 1990) and melts with initially CI chondritic proportions of major element oxides (Wang et al., 2001).

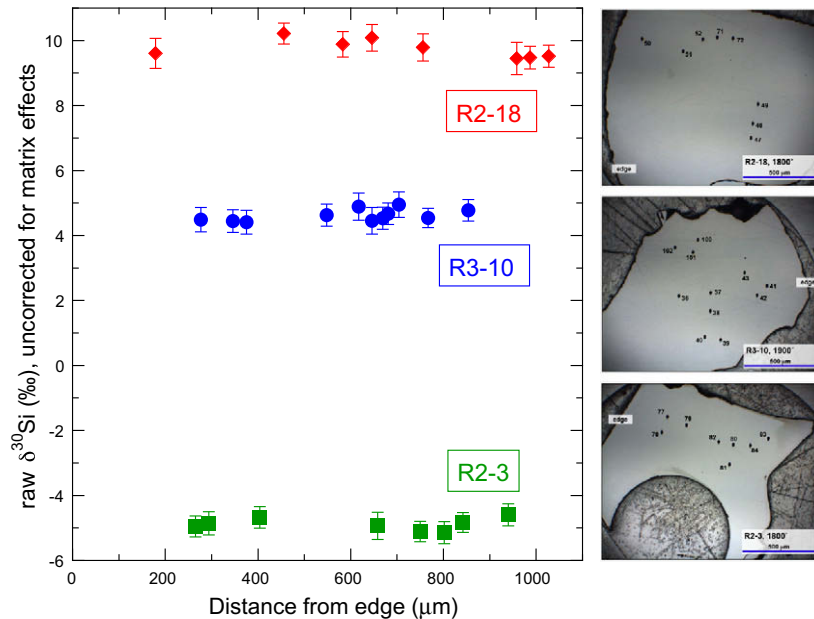


Fig. 6. $\delta^{30}\text{Si}$ vs. distance from sample edge. The data shown are not corrected for matrix effects, but since each sample is chemically uniform, matrix effects will not cause internal variations in $\delta^{30}\text{Si}$ within individual samples. Individual analysis locations are shown in postanalysis reflected light photographs of three representative samples. No systematic internal isotopic fractionation is seen.

fractionation factors reported by Davis et al. (1990) and Wang et al. (2001) in that the samples used in their experiments were several times larger than the ones used in the present study. The presence of iron and magnesium may play a

significant role on the compositional dependence of α_{Si} , although further experiments are clearly needed. Selecting α_{Si} appropriate to the compositions being studied, however, is necessary for understanding fractionation in silicate

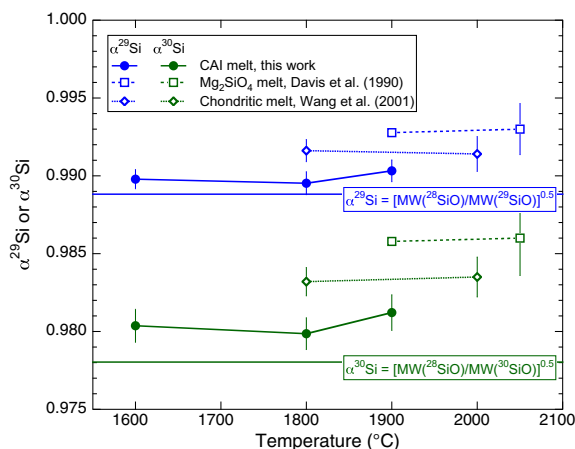


Fig. 7. Experimentally determined α_{Si} values from several studies carried out at different temperatures and using different initial starting compositions. Uncertainties are 2σ . Although no strong dependence of α_{Si} on temperature is apparent for any particular composition, there does appear to be a significant effect of composition on α_{Si} , with α_{Si} values approaching the values calculated from inverse square root of masses of SiO in the order: (1) Mg_2SiO_4 melt; (2) melts of initially CI chondritic composition; and (3) melts of CAI composition.

systems and the experiments reported here are appropriate for studying CAI evaporation.

The lack of temperature dependence of $\alpha_{29\text{Si}}$ and $\alpha_{30\text{Si}}$, combined with a significant dependence on the composition of the evaporating liquid is unlike what has been reported for the kinetic isotope fractionation factor for magnesium. Richter et al. (2007a) have shown that $\alpha_{25\text{Mg}}$ becomes closer to 1 (less fractionating) as the temperature decreases from 1900 to 1600 °C. Once this temperature effect is taken into account, the values of $\alpha_{25\text{Mg}}$ reported by Davis et al. (1990) for liquid Mg_2SiO_4 and by Wang et al. (2001) for a liquid with initially solar proportions of the major oxides are the same, within stated errors, as the value found by Richter et al. (2007a) for CAI-like liquids. Another difference between the kinetic isotope fractionation factors of silicon and magnesium for CAI-like liquids is that the measured $\alpha_{29\text{Si}} = 0.98985 \pm 0.00044$ is quite close to that calculated from $\sqrt{\text{M.W.}(^{28}\text{SiO})/\text{M.W.}(^{29}\text{SiO})} = 0.98883$. In the case of magnesium, where dominant gas species is Mg, the measured values of $\alpha_{25\text{Mg}}$ reported by Richter et al. (2007a), 0.9861 to 0.9882, are significantly different from that calculated $\sqrt{\text{A.W.}(^{24}\text{Mg})/\text{A.W.}(^{25}\text{Mg})} = 0.9798$.

Recondensation can potentially cause additional complications to isotopic fractionation effects preserved in an evaporating liquid. However, Richter et al. (2007a) demonstrated that recondensation had a negligible effect on the values of $\alpha_{25\text{Mg}}$ they measured, and that the difference between the measured $\alpha_{25\text{Mg}}$ and that calculated from $\sqrt{\text{A.W.}(^{24}\text{Mg})/\text{A.W.}(^{25}\text{Mg})}$ is real and has to be taken into account when interpreting the magnesium isotopic fractionation of CAIs. Because we used the same evaporation residues as Richter et al. (2007a), the argument that recondensation effects are negligible applies to the values of $\alpha_{29\text{Si}}$ and $\alpha_{30\text{Si}}$ reported here.

4.2. CAI precursors

The motivation for experiments to determine the kinetic isotope fractionation factor for silicon evaporating from a CAI-like liquid comes from the need for such data to interpret the amount of silicon that must have been lost from a given CAI to account for its silicon isotopic fractionation. We can rewrite Eq. (1) as

$$f_{28\text{Si}} = (R/R_0)^{-\frac{1}{1-\alpha_{29\text{Si}}}} \quad (3)$$

where $R/R_0 = \delta^{29\text{Si}}/1000 + 1$. Thus, given the $\delta^{29\text{Si}}$ of a CAI and an appropriate value for $\alpha_{29\text{Si}}$, one can calculate $f_{28\text{Si}}$ using Eq. (3) and the fraction of total silicon remaining. The fraction of total silicon lost f_{Si} can be calculated from:

$$f_{\text{Si}} = f_{28\text{Si}}(1 + (F_{29}\delta^{29\text{Si}}/1000) + (F_{30}\delta^{30\text{Si}}/1000)), \quad (4)$$

where F_{29} and F_{30} are the fractions of ^{29}Si and ^{30}Si in normal terrestrial silicon, 0.046853 and 0.030924, respectively (Coplen et al., 2002). The equivalent relationships for magnesium are

$$f_{24\text{Mg}} = (R/R_0)^{-\frac{1}{1-\alpha_{25\text{Mg}}}} \quad (5)$$

where $R/R_0 = \delta^{25\text{Mg}}/1000 + 1$, and

$$f_{\text{Mg}} = f_{24\text{Mg}}(1 + (F_{25}\delta^{25\text{Mg}}/1000) + (F_{26}\delta^{26\text{Mg}}/1000)), \quad (6)$$

where F_{25} and F_{26} are 0.10003 and 0.11005, respectively (Catanzaro et al., 1966). Since excess ^{26}Mg could result from ^{26}Al decay, it is assumed that in mass fractionation, $\delta^{26}\text{Mg}$ is twice $\delta^{25}\text{Mg}$ (whether this factor exactly two or not has a negligible effect on the total fraction of magnesium remaining).

Richter et al. (2007a) showed that $\alpha_{25\text{Mg}}$ is temperature dependent and plotted $1000(1 - \alpha_{25\text{Mg}})$ vs. reciprocal temperature, as is appropriate for a kinetically controlled process. We have plotted the Richter et al. (2007a) data and $1000(1 - \alpha_{29\text{Si}})$ vs. reciprocal temperature in Fig. 8 and compared silicon and magnesium evaporation behavior. Taking into account that the Type B CAIs were most likely evaporated at temperatures close to the liquidus temperature of about 1400 °C (Stolper, 1982), the best value to use for $\alpha_{25\text{Mg}}$ is 0.9908 ± 0.0006 (Fig. 8). There is no measurable temperature dependence to $\alpha_{29\text{Si}}$, so we simply adopt the value determined from data collected at all temperatures, 0.98985 ± 0.00044 .

The quantitative relationships between the degree of silicon and magnesium isotopic fractionation and the amount of silicon and magnesium evaporated can be used in a variety of ways to constrain the origin and evolution of CAIs such as the Type B CAIs, whose igneous textures indicate high degrees of partial melting and whose mass-dependent fractionation of silicon and magnesium isotopes suggest that these elements were significantly volatilized while the precursor was partially molten. For example, given estimates of the amount of silicon and magnesium evaporated, one can use the laboratory determined evaporation kinetics of these elements from CAI-like liquids (Richter et al., 2002, 2007a) to constrain their thermal history. A typical conclusion of this sort of exercise is that the Type B CAIs

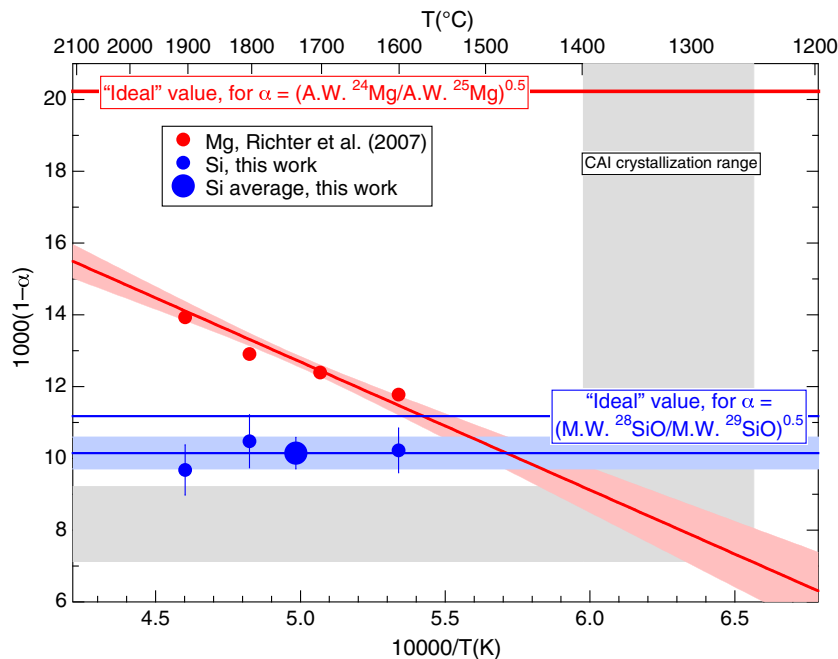


Fig. 8. Relationship between $\alpha_{25\text{Mg}}$, $\alpha_{29\text{Si}}$ and reciprocal temperature for CAI melts; α values are expressed as $1000(1 - \alpha)$. Uncertainties are 2σ . The data for magnesium show a clear temperature effect that allows extrapolation to the crystallization temperature range of Type B CAIs (shown in light gray). The silicon data does not show any temperature dependence, so we adopted the average value obtained from all experiments at all temperatures. For the ideal values, A.W. refers to the atomic weight of the magnesium isotopes and M.W. refers to the molecular weights of the SiO isotopomers.

were partially molten for a time of the order of a few tens of hours (see Richter et al. (2002, 2006), Davis and Richter (2007) and references therein). One would arrive at this conclusion whether one used silicon or magnesium in the analysis.

The greatest uncertainty in arriving at a precise thermal history is not, however, the exact value of the kinetic isotope fractionation factor used to derive the amount of silicon or magnesium lost. The largest uncertainties in determining thermal histories for CAIs involve the effect on the evaporation kinetics of the pressure and composition of the gas surrounding the evaporating materials. When that gas is solar in composition (*i.e.*, mainly hydrogen), the evaporation rates of silicon and magnesium will be increased by about two orders of magnitude at a pressure of 10^{-3} bars of H_2 , compared to the rate in vacuum at the same temperature (Richter et al., 2002). The hydrogen pressure dependence on evaporation rate and α has been preliminarily explored for magnesium (Richter et al., 2002, 2008). Thus far, the effects of significant hydrogen ($P > 10^{-7}$ bars) have been shown to have only minor effects on α , while increasing evaporation rates. The uncertainty in the evaporation kinetics translates into uncertainty in the duration of the high temperatures that melted the Type B CAIs from about 1 h to about 100 h. Even with large uncertainties, this range of times still indicates that the melting of the precursors of the Type B CAIs was the result of one or more brief episodes of transient heating.

The real need for precise determinations of both $\alpha_{29\text{Si}}$ and $\alpha_{25\text{Mg}}$ arises when one wants to calculate the composi-

tion of the precursor of the Type B CAIs, which are the key to addressing such questions as whether the precursors might have been original condensates from a solar composition gas (see Grossman et al. (2000), Simon and Grossman (2004), Richter et al. (2007a), and Grossman et al. (2008), for examples of this approach). We illustrate this approach by using Eqs. (3)–(6) to calculate the fraction of silicon and magnesium lost by a set of CAIs with measured bulk chemical and silicon and magnesium isotopic compositions (Grossman et al., 2008). We then calculate the composition of the precursor for each by adding back to the best estimate of their present composition the lost silicon and magnesium, assuming that the refractory CaO and Al_2O_3 did not evaporate to any significant degree. Somewhat surprisingly, the main source of uncertainty in this approach derives from uncertainties in the actual bulk composition of CAIs. The problem arises because of the highly irregular distribution of minerals in coarse-grained CAIs. Compositions measured by instrumental neutron activation analysis (INAA) on small chips or by electron microprobe measurements on a particular polished surface can be quite different from that of the bulk CAI. One indication of this problem is that many of the reported CAI compositions do not have the solar Ca/Al ratio. The likely reason for this is too much or too little spinel in the chip or surface analyzed. In Grossman et al. (2000), adjustments of the bulk composition of a set of CAIs were made by adding or removing spinel to the extent needed make the bulk composition have solar Ca/Al. These recalculated bulk compositions are called spinel-corrected bulk compositions to

distinguish them from the measured compositions. Simon and Grossman (2004) and Grossman et al. (2008) used a somewhat more complicated procedure involving addition or subtraction of spinel, pyroxene or melilite to achieve a solar Ca/Al ratio. The CAI compositions we used are from Grossman et al. (2008) and use the latter method. Using the chemical and isotopic data presented in Grossman et al. (2008), we calculated precursor compositions by adding back SiO₂ and MgO as determined from the degree of isotopic fractionation of silicon and magnesium (Fig. 9). We show two scenarios: (1) using $\alpha_{29\text{Si}}$ and $\alpha_{25\text{Mg}}$ values calculated from the inverse square root of masses of Mg and SiO; and (2) using our recommended $\alpha_{29\text{Si}}$ and $\alpha_{25\text{Mg}}$ values for 1400 °C, the liquidus temperature of Type B CAIs. Precursor compositions calculated by these two methods are compared with a condensation trajectory for a gas of solar composition at 10⁻³ atm in Fig. 9. Use of the “ideal” values for $\alpha_{29\text{Si}}$ and $\alpha_{25\text{Mg}}$ gives precursor compositions that tend to fall to the magnesium-poor side of this condensation trajectory. The calculated precursor compositions using measured $\alpha_{29\text{Si}}$ and $\alpha_{25\text{Mg}}$ are generally more magnesium-rich and closer to the condensation trajectory, but scatter significantly more than precursor compositions calculated using the “ideal” α values. The application of the empirical value of α places four of the eight Type B CAI precursor compositions on or very close to the calculated condensation tra-

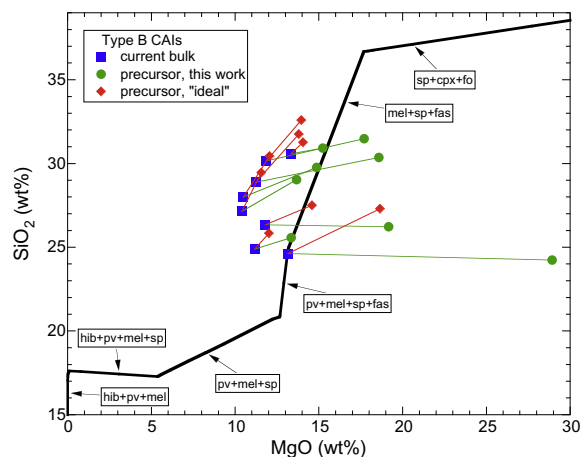


Fig. 9. The precursor compositions for Type B CAIs were calculated from present day bulk compositions (adjusted to the solar Ca/Al ratio) and magnesium and silicon isotopic compositions using two scenarios. (1) Use of “ideal” $\alpha_{25\text{Mg}}$ and $\alpha_{29\text{Si}}$ values based on inverse square root of the masses of Mg and SiO tends to leave data to the left of the condensation trajectory. (2) Using measured $\alpha_{25\text{Mg}}$ extrapolated to 1400 °C and measured $\alpha_{29\text{Si}}$ tends to bring compositions closer to the condensation trajectory, although significant scatter remains. All data for chemical compositions and magnesium and silicon isotopic compositions were taken from Grossman et al. (2008). The condensation trajectory is taken from the same calculation used to construct Fig. 15 in Davis and Richter (2007) and is for a gas of solar composition at a total pressure of 10⁻³ atm. Grossman et al. (2008) have shown that the position of the condensation trajectory can change with pressure and dust/gas ratio. Each segment of the condensation trajectory is labeled with the condensing phase assemblage (hib, hironite; pv, perovskite; mel, melilite; sp, spinel; fas, fassaite; fo, forsterite).

jectory. The remaining four precursor compositions, however, plot to the right of the condensation trajectory, implying a starting composition of excess MgO or depleted SiO₂ relative to expectations. Part of this disagreement may reflect uncertainty in bulk chemical compositions. There are also uncertainties in the location of the condensation trajectory: Grossman et al. (2008) have shown that the position of the condensation trajectory in a SiO₂ vs. MgO plot varies with pressure for a gas of solar composition and that enhanced dust/gas ratios relative to solar composition can also move the condensation trajectory.

Shahar and Young (2007) recently suggested an interesting alternative approach for determining certain aspects of the bulk composition of the precursor of a CAI that does not require specifying the present composition of the CAI. Their approach requires that there be a known unique relationship between the composition of the precursor and the silicon and magnesium composition of the evaporation residue. They tested this idea by considering a range of potential precursor compositions for the Type A CAI Leoville 144A and calculating the elemental and isotopic evolution of each potential precursor by evaporation in order to find which of the precursors ended up with the measured average silicon and magnesium isotopic composition of Leoville 144A. By this approach, they determined that the precursor to Leoville 144A had 23 ± 2 wt% SiO₂ and 15 ± 2 wt% MgO, with the balance being CaO + Al₂O₃ in unconstrained relative proportions. The method also yields an estimate of the present SiO₂, MgO, and CaO + Al₂O₃ of the Leoville 144A. In order for this method to recover accurate compositions, high precision is required when specifying the trajectory in composition space of evaporation residues using a thermodynamic model and appropriate evaporation coefficients for silicon and magnesium. The accuracy of this method also depends on knowing, with high precision, appropriate kinetic isotope fractionation factors used in calculating the associated isotopic fractionations.

We have discussed the need for experimentally determined kinetic fractionation factors, presented our experimental results on evaporated CAI-like liquids, and related this result specifically to the calculation of the composition of Type B CAI precursors. While any temperature dependences of α_{Si} appear negligible in this context, we note the need for experimentally determined, compositionally appropriate silicon isotopic fractionation factors for use in application to other compositions of evaporating liquids. We also point out that our task of providing these high-precision kinetic isotope fractionation factors for silicon and magnesium evaporating from a CAI-like liquid is not yet complete. It remains unknown as to how finite hydrogen pressures might modify the results obtained so far from vacuum evaporation residues. Experiments such as these will continue to provide a basis for constraining processes in the early solar system through the CAI record.

ACKNOWLEDGMENTS

This work was supported by the NASA Cosmochemistry Program through grants NNG06GF19G (AMD, KBK) and

NNG06GE85G (RAM, FMR). The WiseSIMS ion microprobe facility is partially supported by NSF grants EAR03-19230 and EAR07-44079 (JWV, NTK). T. Ushikubo is thanked for his optimism and assistance with the isotopic measurements done at the University of Wisconsin, D. Heinz is thanked for the use of his tools for sample preparation, K. Ludwig is thanked for his freely distributed Isoplot program. Constructive reviews by S. Tachibana and an anonymous reviewer are gratefully acknowledged.

REFERENCES

- Basile-Doelsch I., Meunier J. D. and Parron C. (2005) Another continental pool in the terrestrial silicon cycle. *Nature* **433**, 399–402.
- Catanzaro E. J., Murphy T. J., Garner E. L. and Shields W. R. (1966) Absolute isotopic abundance ratios and atomic weights of magnesium. *J. Res. Natl. Bur. Stand.* **70A**, 453–458.
- Clayton R. N., Hinton R. W. and Davis A. M. (1988) Isotopic variations in the rock-forming elements in meteorites. *Phil. Trans. Royal Soc. Lond. A* **325**, 483–501.
- Coplen T. B., Böhlke J. K., De Bièvre P., Ding T., Holden N. E., Hopple J. A., Krouse H. R., Lamberty A., Peiser H. S., Révész K., Rieder S. E., Rosman K. J. R., Roth E., Taylor P. D. P., Vocke, Jr., R. D. and Xiao Y. K. (2002) Isotope-abundance variations of selected elements. *Pure. Appl. Chem.* **74**, 1987–2017.
- Davis A. M. and Richter F. M. (2007) Condensation and evaporation of solar system materials. In *Meteorites, Planets, and Comets* (ed. A. M. Davis), vol. 1 *Treatise on Geochemistry*, 2nd ed. (eds. H. D. Holland and K. K. Turekian), Elsevier, Oxford, <http://www.sciencedirect.com/science/referenceworks/9780080437514>.
- Davis A. M., Hashimoto A., Clayton R. N. and Mayeda T. K. (1990) Isotope mass fractionation during evaporation of Mg₂SiO₄. *Nature* **347**, 655–658.
- Floss C., El Goresy A., Zinner E., Kransel G., Rammensee W. and Palme H. (1996) Elemental and isotopic fractionations produced through evaporation of the Allende chondrite: implications for the origin of HAL-type hibonite inclusions. *Geochim. Cosmochim. Acta* **60**, 1975–1997.
- Grossman L., Ebel D. S., Simon S. B., Davis A. M., Richter F. M. and Parsad N. M. (2000) Major element chemical and isotopic compositions of refractory inclusions in C3 chondrites: the separate roles of condensation and evaporation. *Geochim. Cosmochim. Acta* **64**, 2879–2894.
- Grossman L., Simon S. B., Rai V. K., Thiemens M. H., Hutcheon I. D., Williams R. W., Galy A., Ding T., Fedkin A. V., Clayton R. N. and Mayeda T. K. (2008) Primordial compositions of refractory inclusions. *Geochim. Cosmochim. Acta* **72**, 3001–3021.
- Hashimoto A. (1990) Evaporation kinetics of forsterite and implications for the early solar nebula. *Nature* **347**, 53–55.
- Janney P. E., Richter F. M., Davis A. M., Mendybaev R. A. and Wadhwa M. (2005) Silicon isotope ratio variations in CAI evaporation residues measured by laser ablation multicollector ICPMS. *Lunar Planet. Sci.* **36**, #2123 (CD-ROM).
- Kita N. T., Ushikubo T., Fu B. and Valley J. W. (2009) High precision SIMS oxygen isotope analysis and the effect of sample topography. *Chem. Geol.* **264**, 43–57.
- Ludwig K. R. (1992) User's manual for Isoplot 3.00: a geochronological toolkit for Microsoft Excel. *Berkeley Geochronol. Center Spec. Pub.* **4**, 1–71.
- Mendybaev R. A., Richter F. M. and Davis A. M. (2006) Crystallization of melilite from CMAS liquids and the formation of the melilite mantle of Type B1 CAIs: experimental simulations. *Geochim. Cosmochim. Acta* **70**, 2622–2642.
- Nagahara H. and Ozawa K. (1996) Evaporation of forsterite in H₂ gas. *Geochim. Cosmochim. Acta* **60**, 1445–1459.
- Nichols R. H., Wasserburg G. J. and Grimley R. T. (1995) Evaporation of forsterite: identification of gas-phase species via Knudsen cell mass spectrometry. *Lunar Planet. Sci.* **26**, 1047–1048.
- Page F. Z., Ushikubo T., Kita N. T., Riciputi L. R. and Valley J. W. (2007) High-precision oxygen isotope analysis of picogram samples reveals 2 μm gradients and slow diffusion in zircon. *Amer. Min.* **92**, 1772–1775.
- Richter F. (2004) Timescales determining the degree of kinetic isotope fractionation by evaporation and condensation. *Geochim. Cosmochim. Acta* **68**, 4971–4992.
- Richter F. M., Davis A. M., Ebel D. S. and Hashimoto A. (2002) Elemental and isotopic fractionation of Type B CAIs: experiments, theoretical considerations, and constraints on their thermal evolution. *Geochim. Cosmochim. Acta* **66**, 521–540.
- Richter F. M., Mendybaev R. A. and Davis A. M. (2006) Conditions in the protoplanetary disk as seen by the type B CAIs. *Meteorit. Planet. Sci.* **41**, 83–93.
- Richter F. M., Janney P. E., Mendybaev R. A., Davis A. M. and Wadhwa M. (2007a) Elemental and isotopic fractionation of Type B CAI-like liquids by evaporation. *Geochim. Cosmochim. Acta* **71**, 5544–5564.
- Richter F. M., Teng F.-Z., Mendybaev R. A., Davis A. M. and Georg R. B. (2008) Elemental and isotope fractionation of CAI-like liquids by evaporation in low pressure H₂. *Lunar Planet. Sci.* **39**, 1385 (CD-ROM).
- Shahar A. and Young E. D. (2007) Astrophysics of CAI formation as revealed by silicon isotope LA-MC-ICPMS of an igneous CAI. *Earth Planet. Sci. Lett.* **257**, 497–510.
- Simon S. B. and Grossman L. (2004) A preferred method for the determination of bulk compositions of coarse-grained refractory inclusions and some implications of the results. *Geochim. Cosmochim. Acta* **68**, 4237–4248.
- Stolper E. (1982) Crystallization sequences of Ca–Al-rich inclusions from Allende: an experimental study. *Geochim. Cosmochim. Acta* **46**, 2159–2180.
- Stolper E. and Paque J. M. (1986) Crystallization sequences of Ca–Al-rich inclusions from Allende: the effects of cooling rate and maximum temperature. *Geochim. Cosmochim. Acta* **50**, 1785–1806.
- Wang J., Davis A. M., Clayton R. N. and Hashimoto A. (1999) Evaporation of single crystal forsterite: evaporation kinetics, magnesium isotope fractionation, and implications of mass-dependent isotopic fractionation of a diffusion-controlled reservoir. *Geochim. Cosmochim. Acta* **63**, 953–966.
- Wang J., Davis A. M., Clayton R. N., Mayeda T. K. and Hashimoto A. (2001) Chemical and isotopic fractionation during the evaporation of the FeO–MgO–SiO₂–CaO–Al₂O₃–TiO₂–REE melt system. *Geochim. Cosmochim. Acta* **65**, 479–494.